

1
2
3 Mechanical and physicochemical characterization along with
4 biological interactions of a new Ti25Nb21Hf alloy for bone tissue
5 engineering
6
7

8 C. Herranz-Diez, F. J. Gil, J. Guillem-Marti, J.M. Manero(*)
9

10 ^a Biomaterials, Biomechanics and Tissue Engineering Group, Department of Materials Science and
11 Metallurgy, Technical University of Catalonia (UPC), ETSEIB, Av. Diagonal 647, 08028 Barcelona,
12 Spain
13

14 ^b Biomedical Research Networking Centre in Bioengineering, Biomaterials and Nanomedicine (CIBER-
15 BBN), Campus Río Ebro, Edificio I+D Bloque 5, 1^a planta, C/ Poeta Mariano Esquillor s/n, 50018
16 Zaragoza, Spain
17

18 ^c Centre for Research in NanoEngineering (CRNE) – UPC, C/Pascual i Vila 15, 08028 Barcelona, Spain
19
20
21
22
23

24 *Corresponding author:
25
26

27 Dr. J.M. Manero:
28

29 Biomaterials, Biomechanics and Tissue Engineering Group, Department of Materials Science and
30 Metallurgy, Technical University of Catalonia (UPC), ETSEIB, Av. Diagonal 647, 08028 Barcelona,
31 Spain.
32

33 E-mail address: jose.maria.manero@upc.edu
34
35
36
37
38
39
40
41
42
43
44
45
46
47
48
49
50
51
52
53
54
55
56
57
58
59
60

ABSTRACT

Nowadays, one of the main challenges in metal implants for bone substitution is the achievement of an elastic modulus close to that of human cortical bone as well as to provide an adequate interaction with the surrounding tissue avoiding *in vivo* foreign body reaction. From this perspective, a new Ti-based alloy has been developed with Nb and Hf as alloying elements which are known as non-toxic and with good corrosion properties. The microstructure, mechanical behaviour and the physicochemical properties of this novel titanium alloy have been studied. Relationship of surface chemistry and surface electric charge with protein adsorption and cell adhesion have been evaluated due to its role for understanding the mechanism of biological interactions with tissues. The Ti25Nb21Hf alloy presented a lower elastic modulus than commercial alloys with a superior ultimate strength and yield strength than CP-Ti and very close to Ti6Al4V. It also exhibited good corrosion resistance. Furthermore, the results revealed that it had no cytotoxic effect on rat mesenchymal stem cells and allowed protein adsorption and cell adhesion. The experimental results make this alloy a promising material for bone substitution or for biomedical devices.

Keywords:

Titanium based alloy, cell adhesion, protein adsorption, electrochemical behavior, contact angle, *in vitro* cell culture

1. Introduction

Metallic materials are used in a variety of biomedical devices and are remarkably important for bone substitution to improve the quality of life (QOL) of the patient¹. The materials currently used for surgical implants include 316L stainless steel (316LSS), cobalt chromium (Co–Cr) alloys and titanium (Ti) and its alloys. However, chemical elements such as Ni, Cr and Al are found to be released from these alloys due to corrosion². A protective oxide layer is typically generated on these alloys acting as a barrier against chemical attack and corrosion, although this oxide layer can be depleted by wear, corrosion or fatigue. These processes produce the release of ions or wear debris which may cause some allergic reaction and biocompatibility problems³⁻⁵. For instance, the low wear resistance of Ti6Al4V alloy has been demonstrated to induce the release of aluminium (Al) and vanadium (V) ions which are potentially hazardous for human body⁶. Therefore, these elements are now avoided as much as possible as an additive in metallic biomaterials.

Moreover, another main goal in implantology is to replace bone, or tooth, with materials that exhibit a low elastic modulus near to that of human bone without having undesirable reactions. The elastic modulus of bone is 14-20 GPa⁷ while most of the materials used are in the range of 110-240 GPa⁸. This mismatch of the elastic modulus produces stress shielding that eventually leads to implant failure. Bone requires a mechanical stimulus for remodeling; hence, in a bone-implant coupling, it is essential to use materials with rigidity properties similar to bone for improving the load-transfer and favoring bone healing and remodeling^{9,10}.

Among metallic biomaterials, Ti is still the most commonly used biomaterial in implantology due to its high strength, high corrosion resistance, low elastic modulus, chemical stability and biocompatibility¹¹. However, a considerable number of bone replacements end with implant failure mainly due to the poor wear resistance and the high elastic modulus of Ti (110 GPa), which is still far from the above mentioned for bone. Thus the development of Ti alloys with excellent combination of high strength and low elastic modulus similar to bone values to replace traditional medical metallic alloys are required.

1
2
3 Due to the lower elastic modulus exhibited by the β (BCC) phase of Ti and its good workability
4 compared with the values presented by the α (HCP) phase^{12,13}, β Ti alloys are a relevant field of
5 investigation¹⁴⁻¹⁶. However, the β phase in Ti is only achieved at high temperature. Then, in order to
6 stabilize this phase at low temperature and to reduce the elastic modulus of Ti, nontoxic and non-
7 allergic β -stabilizing alloying elements such as Ta, Nb, Mo, Hf, and, in some cases Zr as a neutral
8 element, are used. Several efforts have been concentrated on the production of natively biocompatible
9 alloys; e.g. the Ti-Nb and the related Ti-Nb-X system (where X = Zr, Ta, Au, O) have yielded alloys
10 with superelastic strains as high as 4.2%, sufficient for most applications¹⁷⁻¹⁹ without affecting
11 biocompatibility. Noteworthy, the TiNbHf ternary system presents very interesting properties.
12 Previous studies in our research group^{20,21} showed a decrease in the apparent elastic modulus up to 42
13 GPa for Ti-16.2Hf-24.8Nb alloy by increasing the cold work percentage. Moreover, in vitro
14 citotoxicity tests, hemolysis tests and platelet tests showed low citotoxicity and excellent hemo-
15 compatibility for TiNbHf systems²².

16
17
18
19
20
21
22
23
24
25
26
27
28
29 Some authors have used a method based on molecular orbital theory introduced by Morinaga *et al.* for
30 designing low elastic modulus alloys²³. The resulting properties predictive map was based on two
31 parameters: the average of the bond orders between the alloying elements and the original element
32 (Bo) and the mean energy of the lowest virtual d-orbitals (Md). In the previous study by our research
33 group, this prediction map has been improved by using more precise parameters to design low elastic
34 modulus alloys¹⁴. In one hand, the bond orders were improved calculating from a natural population
35 analysis (BO)²⁴. On the other hand, the energy of occupied orbitals centred in the alloying element
36 (OE) was used instead of the energy of virtual *d*-orbitals. From the resulting map, a Ti alloy
37 presenting 25 wt.% niobium (Nb) and 21 wt.% hafnium (Hf) was selected for the present study.

38
39
40
41
42
43
44
45
46
47
48 In addition to mechanical properties, superficial implant properties are also very important for tissue
49 integration. Among these properties, wettability and superficial charge are related to the material
50 chemical composition and mediate the tissue-implant interaction through protein adsorption.
51 Wettability, generally referred as hydrophobicity/hydrophilicity, is defined as the capacity of a surface
52 to attract or repulse liquid. Although wettability affects protein adsorption, observations regarding this
53 effect have not always been consistent²⁵. The electric charge of a material surface, measured as zeta-
54
55
56
57
58
59
60

potential, indicates which entities would be attracted. Negative values of zeta-potential indicate negative surface charge which would attract cations and positively charged proteins while positive values indicate a positively charged surface that would attract negatively charged particles.

The present work aims to study the mechanical, physicochemical and biological properties of a new Ti alloy, Ti25Nb21Hf, designed from the predictive map previously developed in our research group. To achieve this objective, the mechanical and superficial properties of the new Ti alloy were analyzed and compared to those of two commonly used implant biomaterials, Ti and Ti6Al4V. In addition, the protein adsorption and cellular adhesion were also evaluated *in vitro*.

2. Materials and methods

2.1. Alloy design and sample preparation

A titanium-25 wt.% niobium- 21 wt.% hafnium alloy was produced based on optimization of molecular orbital calculations of electronic structures¹⁴ towards low modulus of elasticity and the potential for superelasticity. From this predictive map, the selected alloy has an average valence electron number (e/a) of 4.176. This value is near to the one reported by Hao et al.²⁶, who recommended it in order to obtain a low elastic modulus. Moreover, the alloy presents a bond order (BO) of 0.61212 eV and an orbital free energy (OE) of 0.15260 eV which are similar to those obtained by M. Gonzalez et al^{20,21}.

The new alloy was fabricated at *Fort Wayne Metals Research Corporation (Fort Wayne, Indiana, USA)*. Bars of diameter 10 mm and longitude 300 mm were obtained by means of vacuum arc melting (VAM) and drop casting. The bar was vacuum-homogenized and annealed at 650 °C. Commercially pure grade 2 titanium (CP-Ti) and Ti6Al4V bars were purchased from Outokumpu (Finland) fulfilling the ASTM F 67 standard. Discs of 2 mm in thickness were cut from CP-Ti, Ti6Al4V and Ti25Nb21Hf. They were polished using 600 and 1,200 grit silicon carbide (SiC) abrasive papers and finally, they were further polished with napped polishing pads with a colloidal silica polishing abrasive (1 and 0.05 μm).

2.2. Microstructure analyses

Crystallographic studies were carried out by X-ray diffraction (XRD) technique (Diffractometer D8 Advance, Bruker, Billerica, MA, USA) operated at 40 Kv, 30 mA and $\text{CuK}\alpha$ ($\lambda=1.542 \text{ \AA}$) radiation. TEM samples were prepared by the jet-polishing method using Tenupol-3 equipment (Struers, Denmark) in a solution of 350 mL 2-butoxiethanol, 60 mL perchloric acid and 350 mL methanol at 10°C and 40 V. Thin foils were analyzed by TEM using a JEM 1200 EXII (JEOL, Tokyo, Japan).

2.3. Mechanical tests

Tensile specimens of CP-Ti, Ti6Al4V and Ti25Nb21Hf were machined according to ASTM E8M-04. Tensile tests were performed using an Instron 8500 testing machine (Instron, Norwood, MA, USA) at $1.5 \times 10^{-4} \text{ s}^{-1}$ strain rate. All mechanical tests were repeated six times. The main mechanical properties were determined: ultimate tensile strength (σ_{max}), yield strength (σ_y) and the elastic modulus (E).

2.4. Corrosion studies

Electrochemical measurements were performed using a PARSTAT 2273 potentiostat (Princeton Applied Research, Princeton, NJ, USA) in a standard three electrode-setup containing a saturated calomel electrode (SCE) as the reference electrode, a graphite electrode as cathode and specimen (0.78 cm^2 for CP-Ti and Ti25Nb21Hf and 1.32 cm^2 for Ti6Al4V exposed area) as working electrode. Experiments were performed in Hank's Balanced Salt Solution (HBSS; Sigma-Aldrich) at 37°C . Specimens were embedded in resin, ultrasonically cleaned in ethanol for 15 min and immersed into the electrolyte solution. Upon immersion of the specimens into the electrolyte, the open-circuit potential (E_{oc}) was measured for two hours and the data was recorded each second. Subsequently, potentiodynamic electrochemical measurements were carried out incrementing the voltage from -0.3 to 4 V at a scan rate of 1 mV/s. After that, the voltage was reversed back to the starting value. Assays were monitored by PowerSuite® Electrochemical software. Tafel extrapolation was used to estimate the E_{corr} and I_{corr} values. Open circuit potential and cyclic voltammetry were conducted according to the ISO 10993-15:2009.

2.5. Wettability and surface free energy (SFE)

Contact angles were measured using the sessile drop method with an *Oca 15+* plus (Dataphysics, Germany) and analyzed with the SCA20 software (Dataphysics). Total SFE and dispersive and polar components of SFE were determined obtaining contact angles with two different liquids on each substrate surface: ultrapure distilled water (MilliQ), which is a polar liquid, and di-iodomethane, which is a non-polar liquid. A series of at least three drops (3 μl /drop) were used in triplicate at room temperature in a saturated environmental chamber. The surface energy was calculated from contact angles (θ) according to the Owens and Went approach²⁷:

$$\gamma_l(1 + \cos \theta) = 2 \sqrt{\gamma_s^d \gamma_l^d} - 2 \sqrt{\gamma_s^p \gamma_l^p} \quad (\text{equation 1})$$

where γ^d and γ^p are the dispersive and polar components of SFE, respectively, for solid (s) and liquid (l).

2.6. Z-potential

The Z-potential was measured using a SurPASS Electrokinetic Analyzer (Anton Paar ; Graz, Austria). A 1 mM KCl solution was used as electrolyte. The electrolyte solution was adjusted to a starting pH = 8.0 and automatic titration was performed down to pH = 2.0 adding HCl. The apparent Z-potential was calculated using the Fairbrother-Mastin equation²⁸.

$$\zeta = \frac{dU}{dp} \cdot \frac{\eta}{\varepsilon \cdot \varepsilon_0}$$

where dU/dp is the slope of streaming potential versus pressure, η the electrolyte viscosity, ε the relative liquid permittivity, ε_0 the vacuum permittivity and κ the specific conductivity of the bulk electrolyte solution

2.7. Protein adsorption

Human plasma fibronectin (Sigma-Aldrich, purity >95%) was used as model protein in this study. Fibronectin was diluted in phosphate buffered saline (PBS) at 50 $\mu\text{g}/\text{ml}$ and 150 μl were added on each sample. Incubation was performed for 2h at room temperature. Afterwards, non-adherent protein concentrations were determined using the Micro BCATM Protein Assay Kit (Thermo Scientific, Illinois, USA) according to manufacturer's instructions. Measurements were performed using an ELx800 universal microplate reader (Bio-Tek Instruments, Inc, Winooski, VT, USA) at $\lambda =$

1
2
3 562nm. The quantity of adsorbed protein was obtained by subtracting the non-adherent protein from
4 the initial added protein. Measurements were performed in triplicate. Results from each sample were
5 normalized versus their corresponding area.
6
7

8 9 2.8. Cell culture

10 Rat mesenchymal stem cells (rMSC) were extracted from femurs of young Lewis rats and expanded
11 in Advanced DMEM supplemented with 10% fetal bovine serum, 20 mM HEPES buffer solution,
12 penicillin/ streptomycin antibiotics (50 U/ml and 50 µg/ml, respectively) and 2 mM L-glutamine, all
13 from Invitrogen (Carlsbad, CA,USA). Cells were cultured at 37°C in humidified atmosphere with 5%
14 CO₂. Cells from passage 5 were used in all the experiments. For cellular assays, samples were
15 sterilized in 70% ethanol for 30 min followed by three rinses in PBS.
16
17

18 19 2.9. Cytotoxicity

20 The cytotoxic effect was evaluated according to the ISO 10993-5 standard by indirect contact.
21 Samples were incubated for 72h in complete medium and supernatants were collected. This extracts
22 were serial diluted in complete medium (1, 1:1, 1:100 and 1:1000) and transferred to new microplate
23 wells where 5.000 cells were previously seeded. Cells were incubated for 24h, washed with PBS and
24 lysed with 100 µl of M-PER® (Mammalian Protein Extraction Reagent; Thermo Scientific). Viable
25 cells were quantified using the Cytotoxicity Detection Kit^{PLUS} LDH (Roche Applied Sciences,
26 Penzberg, Germany) following the manufacturer's instructions. Measurements were performed in
27 triplicate and optical densities at λ=492nm were obtained. The percentage of viability was calculated
28 using the following formula:
29
30
31
32
33
34
35
36
37
38
39
40
41
42
43
44

$$45 \text{ Viability (\%)} = \frac{\text{experimental value} - \text{negative control}}{\text{positive control} - \text{negative control}} \times 100$$

46
47
48 Where negative control is the tested medium without cells and positive control is cells with complete
49 medium.
50

51 52 2.10. Cell adhesion assay

53 Cells were seeded on samples at a density of 25.000 cells/well and allowed to adhere for 5h. Then,
54 culture medium was removed; cells were washed in PBS and lysed with 300 µl of M-PER®. The
55
56
57
58
59
60

1
2
3 Cytotoxicity Detection Kit ^{PLUS} LDH was used as above described. To express the results in cell
4 number a calibration curve with decreasing number of cells was prepared. Experiments were
5 performed in triplicate and results from each sample were normalized versus their corresponding area.
6
7

8 9 *2.11. Statistical analysis*

10 All data were expressed as mean values \pm standard deviations. Significant differences between groups
11 were analyzed by ANOVA test followed by post-hoc pairwise comparisons using Tukey's test with a
12 significance level set at $p < 0.05$.
13
14
15
16

17 18 19 **3. Results and discussion**

20 21 *3.1. Microstructure*

22 XRD patterns (figure 1) showed a microstructure mainly formed by β -phase with body-centered cubic
23 crystallographic structure as well as a minor phase of martensitic α'' with an orthorhombic structure
24 (S.G. Pcm). The corresponding lattice parameters were $a = 3.319 \text{ \AA}$ for the β phase; and $a = 4.88720$
25 \AA , $b = 3.13210 \text{ \AA}$ and $c = 4.77410 \text{ \AA}$ for the martensitic α'' phase.
26
27
28
29
30

31 Table 1 shows the theoretical crystallographic planes and their corresponding intensities according to
32 the Joint Committee on Powder Diffraction Standards. The two most intense peaks corresponding to
33 α'' martensitic phase (111 and 002) are partially overlapped by the peak 100 of the β phase. However,
34 the (200) peak (third with higher intensity for α'' martensitic phase) can be seen clearly confirming its
35 presence. Since there is a little α'' -phase, the less intense peaks remain masked. Therefore, the second
36 phase detected was identified to be α'' -martensite of C-centered orthorhombic lattice similar to that
37 reported in Ti-Nb binary system. The XRD patterns obtained have a number of similarities with other
38 Ti-Nb^{29,30}, Ti-Nb-Ta³¹ or Ti-Nb-Hf³² alloys studied in the literature.
39
40
41
42
43
44
45
46
47

48 TEM images also demonstrated that the alloy was mainly composed of β -phase equiaxial grains with
49 high dislocation density (Fig. 2). In addition, α'' -martensite was observed inside the β -phase grains. It
50 is well known that the presence of ω -phase precipitates in β matrix could be confirmed by electron
51 diffraction pattern³³. In this case an ω -phase was not observed.
52
53
54
55

56 57 *3.2. Mechanical properties*

58
59
60

1
2
3 The stress-strain results for all the studied materials are shown in Table 2. Both tensile strength (σ_{\max})
4 and yield strength (σ_y) are higher than those of CP-Ti and are very close to the values obtained for
5 Ti6Al4V. Similar results were previously found in a study on the mechanical properties of Ti-Nb
6
7 Ti6Al4V. Similar results were previously found in a study on the mechanical properties of Ti-Nb
8
9 alloys with different contents of Nb²⁹. In that study, authors found that the elastic modulus decreased
10
11 and the tensile strength increased while increasing the proportion of Nb until the formation of an ω -
12
13 phase, at 26% of Nb.

14
15 It is well known that the presence of β -phase in a titanium alloy is associated with a reduction in the
16
17 elastic modulus. In fact, the alloy fabricated in the present study mainly composed of β -phase grains
18
19 exhibited a lower elastic modulus compared with CP-Ti or Ti6Al4V alloy. The obtained elastic
20
21 modulus (85 GPa) is very close to previous values of TiNbHf ternary alloys studied in our research
22
23 group^{20,21}, confirming that addition of Nb and Hf decreases the elastic modulus of CP-Ti.
24
25 Furthermore, these TiNbHf ternary alloys can exhibit very interesting properties since by means of
26
27 severe plastic deformation (SPD) the mechanical properties could be strongly enhanced^{20,21}.

28 29 30 3.3. Corrosion behaviour

31
32 Materials in contact with body fluids get oxidized releasing ions to the surrounding tissue and the
33
34 body stream which can be hazardous³⁴. A material with high corrosion resistance would minimize this
35
36 effect and thus, improve biocompatibility. The corrosion resistance of the Ti25Nb21Hf was evaluated
37
38 using two different methods.

39 40 3.3.1. Open circuit potential

41
42 Fig. 3 shows the open circuit potentials of Ti, Ti6Al4V and Ti25Nb21Hf obtained in HBSS at 37°C.
43
44 All three materials showed a clear active to passive oxidation transition at E_{oc} near to 0 V, which
45
46 evidence the formation of a passive protective oxide layer on the surface of all the samples.
47
48 Noteworthy, the value of E_{oc} for the Ti25NbHf alloy is considerably higher than the E_{oc} value of the
49
50 Ti6Al4V alloy and similar to CP-Ti (Table 3). Higher values of E_{oc} are indicative of higher resistance
51
52 to corrosion under the assay conditions.

53
54 The Ti25Nb21Hf and Ti open circuit potential trends were similar. Both materials exhibited an open
55
56 circuit potential stabilization that was not seen for the Ti6Al4V behaviour. Similar results were found
57
58 in other studies that used niobium and/or hafnium as Ti alloying elements, suggesting that these
59
60

1
2
3 elements did not change the excellent corrosion behaviour of Ti³⁴⁻³⁶. Interestingly, Ti25Nb21Hf
4 presented a higher initial positive slope, stabilizing earlier. This faster oxide layer generation is
5 encouraging for implant purposes³⁸.
6
7

8 9 3.3.2. Cyclic Voltammetry

10 The cyclic voltammetry curves obtained for each material are shown in Fig. 4. The calculated
11 corrosion potential (E_{corr}) for CP-Ti was $E_{\text{corr}} = -59$ mV, for Ti6Al4V was $E_{\text{corr}} = -39$ mV, whereas for
12 Ti25Nb21Hf alloy was $E_{\text{corr}} \approx -124$ mV. The corrosion current density (I_{cc}) values for CP-Ti and
13 Ti6Al4V alloy were similar, whilst the value for Ti25Nb21Hf alloy was lower. All three materials
14 reached their respective stable passive current densities as the potential increased, indicating the
15 existence of a passive layer. No breakdown was observed in either of the materials under study.
16
17

18 Although the E_{corr} value for Ti25Nb21Hf alloy was lower than CP-Ti and Ti6Al4V, the I_{cc} value
19 indicates a good passivation with density value lower than CP-Ti and Ti6Al4V, suggesting that the
20 designed alloy possesses an excellent corrosion resistance. This excellent corrosion behaviour is
21 attributed to the oxide layer formed on the surface due to the presence of, in addition to Ti, Nb and Hf.
22 High quantities of Nb repassivate more quickly and the passive film is more stable than low Nb-
23 containing alloys mainly due to the formation of Nb₂O₅ phase³⁹⁻⁴⁰. Hf has also excellent corrosion
24 behaviour, mainly due to the formation of HfO₂, which generates a stable surface oxide layer similar
25 to Ti⁴¹.
26
27
28
29
30
31
32
33
34
35
36
37
38

39 3.4 Contact angle measurements and SFE calculation

40 Fig. 5a shows the contact angles obtained by the sessile drop method on the different materials. The
41 addition of Nb and Hf decreased the water contact angle of CP-Ti (85°) in the obtained Ti25Nb21Hf
42 alloy (56°). However, this value was higher compared to the Ti6Al4V value (45°). In contrast, the
43 diiodomethane contact angles were similar for CP-Ti and Ti25Nb21Hf alloy, whereas the values
44 observed in Ti6Al4V alloy were lower. The decrease in the ternary alloy contact angles should be
45 attributed to the hydrophilicity properties of Nb⁴² and probably Hf.
46
47
48
49
50
51
52

53 The lower contact angle values obtained for the studied alloy corresponded to a higher SFE compared
54 to CP-Ti, but similar to the Ti6Al4V alloy (Fig. 5b). Although mainly interactions are attributed to
55
56
57
58
59
60

1
2
3 dispersive SFE component, no differences were observed between each surface. Then, differences in
4 the alloy SFE are explained by the higher polar SFE component value compared to Ti value.

5 6 7 *3.5 Zeta potential results*

8
9 Zeta-potential measurements have shown different electrokinetic behaviour in the interactions at the
10 interface between aqueous electrolyte and each material surface studied. Fig. 6a shows zeta-potential
11 values versus pH change for a standard 1mM KCl solution for Ti, Ti6Al4V and Ti25Nb21Hf. The
12 zeta-potential of both alloys gradually decreased while pH increased, whereas zeta-potential of Ti
13 dramatically decreased in the 3-5 pH range. The isoelectric point (IEP) is the pH at which a surface
14 presents no net electrical charge. Ti exhibited the highest IEP value (3.2) whereas Ti6Al4V and
15 Ti25Nb21Hf alloys presented similar IEP values (2.4 and 2.1 respectively).
16
17

18
19 The zeta-potentials for each material at pH 7 are shown in Fig. 6b. The less negative zeta-potential
20 value was observed for the Ti25Nb21Hf alloy. Proteins have a specific electric charge at
21 physiological conditions that depends on their amino acid sequence. In this study, Ti and the studied
22 Ti alloys displayed slightly different surface charge properties. Their influences on protein adsorption
23 could display different behaviour, which will be discussed in the protein adsorption section.
24
25
26
27
28
29
30
31
32

33 *3.4 Cytotoxicity assessment*

34
35 Fig. 7 shows the percentage of cell viability after 24h of culture in different dilutions of medium
36 extracts from each type of sample. The percentage of viable cells in all conditions was above 90%
37 with no statistical significant differences between each condition. Similar results were found in a
38 previous study using other Ti-Nb and Ti-Nb-Hf alloys compositions⁴³. The exposure of cells to
39 different extract concentrations of the new Ti25Nb21Hf alloy demonstrated no cytotoxic effect.
40
41
42
43
44

45 *3.5 Protein adsorption*

46
47 Fig. 8 shows the adsorbed amount of fibronectin on each material. The quantity of fibronectin
48 adsorbed on the Ti25Nb21Hf alloy ($0.81 \mu\text{g}/\text{cm}^2$) was no statistically significant different compared
49 to the adsorbed amount on CP-Ti ($0.86 \mu\text{g}/\text{cm}^2$) and Ti6Al4V alloy ($0.75 \mu\text{g}/\text{cm}^2$). The adsorption of
50 proteins on the surface of a metal mainly depends on the physicochemical characteristics of both
51 interactants. Without considering the effect of roughness, since surfaces were polished in the present
52 study, amphoteric and hydrophilic/hydrophobic characteristics become the most influencing surface
53
54
55
56
57
58
59
60

1
2
3 parameters for protein adsorption⁴⁴. The oxidation of metal surfaces generates hydroxyl groups that
4
5 yield amphoteric characteristics, changing its surface zeta potential as a result of the change in pH. At
6
7 physiological pH, all the tested surfaces presented anionic character suggesting that should attract
8
9 cations or positively charged proteins. Fibronectin is a protein with negative net charge that should be
10
11 repulsed by anionic surfaces. However, in our study fibronectin was well adsorbed on all the studied
12
13 surfaces, without any statistically significant difference. The hydrophilic/hydrophobic character also
14
15 plays an important role on protein adsorption. Although there is considerable diversity of opinion
16
17 regarding protein-adsorption properties of hydrophilic or hydrophobic surfaces⁴⁵, it seems that
18
19 proteins tend to adsorb stronger to non-polar than to polar surfaces⁴⁶. In fact, no statistical significant
20
21 differences were found in the levels of adsorbed fibronectin on the different studied surfaces, which
22
23 presented different SFE values but similar non-polar levels. This could be because the increase in the
24
25 SFE of Ti25Nb21Hf was not enough for enhancing the protein adsorbed on CP-Ti. In addition, it was
26
27 found that fibronectin is able to bind to both hydrophilic and hydrophobic surfaces⁴⁴. Then, our results
28
29 demonstrated that Ti25Nb21Hf alloy is capable to adsorb protein at similar levels than CP-Ti and
30
31 Ti6Al4V.

32 33 3.6 Cell adhesion

34
35 Cell adhesion is mediated by interaction with preadsorbed proteins during implant integration.
36
37 Immediately after implantation, proteins from blood are adsorbed onto the implant surface and favour
38
39 cell adhesion. In order to mimic this process, the cell adhesion assay was performed in medium
40
41 containing FBS, since proteins in the serum were rapidly adsorbed onto the material surface before
42
43 cells adhere. Cell adhesion on the CP-Ti, Ti6Al4V alloy and Ti25Nb21Hf alloy was quantified 4h
44
45 after cell seeding (Fig. 9). The number of cells adhered on the different materials showed no statistical
46
47 significant differences. Although albumin is the most abundant serum protein, it is suspected that after
48
49 adsorption onto moderately hydrophilic surfaces it is displaced by cell adhesive proteins⁴⁷. One of the
50
51 main cell adhesive proteins is fibronectin, which was tested in our study without any differences in
52
53 adsorption levels between the tested surfaces. This finding correlated well with cell adhesion assay,
54
55 having same amounts of cells on each sample surface. Then, it can be concluded that *in vitro*
56
57
58
59
60

1
2
3 biological response of the developed titanium alloy was similar to the commonly used Ti and
4 Ti6Al4V materials.
5
6
7

8 9 **4. Conclusions**

10
11 In this work, the mechanical, physicochemical and biological properties of a new titanium alloy
12 containing niobium and hafnium were investigated. The addition of 25 wt.% Nb and 21 wt.% Hf to
13 CP-Ti resulted in a ternary alloy mainly composed of β -phase grains with α'' -phase martensitic plates.
14
15 Interestingly, the alloy exhibited excellent mechanical properties, considerably decreasing the elastic
16 modulus of the currently used materials for implantation, CP-Ti and Ti6Al4V alloy, and presenting
17 similar tensile strength values than Ti6Al4V. Moreover, this new Ti alloy also exhibited an excellent
18 corrosion resistance, forming a rapid passive oxide layer. In addition, it exhibited a moderately
19 hydrophilic surface and a lower negative surface charge compared to CP-Ti and Ti6Al4V. *In vitro*
20 cytotoxicity assays demonstrated non effects on mesenchymal stem cells viability. Finally, the
21 Ti25Nb21Hf alloy is capable to adsorb fibronectin and to favour cell adhesion at similar values than
22 CP-Ti and Ti6Al4V alloys.
23
24
25
26
27
28
29
30
31
32

33 The interesting mechanical and physicochemical properties of the new developed Ti25Nb21Hf alloy
34 combined with the biological response make it a potential candidate for bone replacement. However,
35 additional studies can be further investigated in order to enhance the mechanical properties. Recently
36 it has been reported that severe plastic deformation techniques (equal channel angular pressing,
37 ECAP, accumulative roll bonding, ARB or high pressure torsion, HPT) are a promising method due to
38 its ability to increase the mechanical strength maintaining a low Young's modulus or even lowering it,
39 in these TiNbHf ternary alloys.
40
41
42
43
44
45
46
47
48

49 **5. Acknowledgements**

50 The authors would like to thank the Spanish Government for financial support through MAT2012-
51 30706 project co-funded by the EU through European Regional Development Funds and the FI
52 fellowship of the AGAUR Agency. Authors would also like to thank the staff of Fort Wayne Metals
53 for their help with material fabrication and Marc Fernández for corrosion experiments assistance.
54
55
56
57
58
59
60

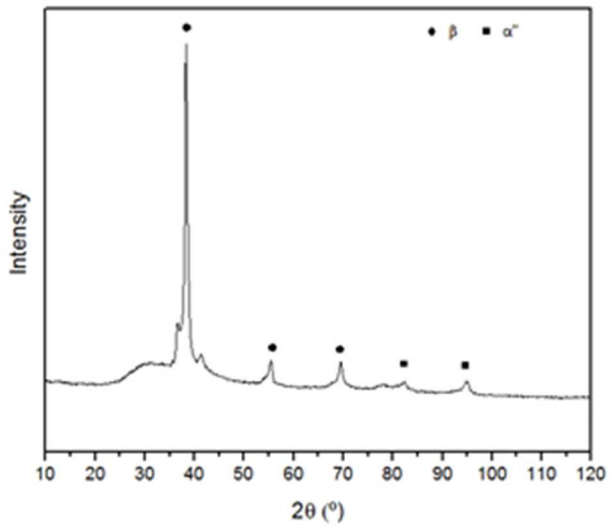
7. REFERENCES

1. M. Niinomi, M. Nakai, J. Hieda. Development of new metallic alloys for biomedical applications. *Acta Biomaterialia* 8 (2012) 3888–3903.
2. O. Yoshimitsu, G.Emiko. On the Effects of Hot Forging and Hot Rolling on the Microstructural Development and Mechanical Response of a Biocompatible Ti Alloy. *Biomaterials* 2005;26:11–21
3. H.H. Huang, H.Y. Chiu, H.T. Lee, H.W. Yang, K.H. Su, and C.C. Hsu, Ion Release from NiTi Orthodontic Wires in Artificial Saliva with Various Acidities, *Biomaterials*, 2003, 24, p 3585–3592.
4. Lu XY, Bao X, Huang Y, Qu YH, Lu HQ, Lu ZH. Mechanisms of cytotoxicity of nickel ions based on gene expression profiles. *Biomaterials* 2009, 30, 141–148.
5. K.Cederbrant, C.Anderson, M.Marcusson, P.Hultman. Cytokine Production, Lymphocyte Proliferation and T-Cell Receptor V β Expression in Primary Peripheral Blood Mononuclear Cell Cultures from Nickel-Allergic Individuals. *Int Arch Allergy Immunol*, 132; 2003, p.373-379.
6. Urban RM, Jacobs JJ, Tomlinson MJ, Gavrilovic J, Black J, Peoc'h M. Dissemination of wear particles to the liver, spleen, and abdominal lymph nodes of patients with hip or knee replacement. *J. Bone Joint Surg Am.* 2000 Apr;82(4):457-76.
7. R. Boyer, G. Welsch, E.W. Collings. *Materials properties handbook. Titanium Alloys.* Ed ASM International. (1994) ISBN: 0-87170-481-1.
8. Geetha M, Singh AK, Asokamani R, Gogia AK. Ti based biomaterials, the ultimate choice for orthopaedic implants – A review. *Prog Mater Sci [Internet]*. 2009;54(3):397–425.
9. Christopher Boyle, Il Yong Kim. Comparison of different hip prosthesis shapes considering micro-level bone remodeling and stress-shielding criteria using three-dimensional design space topology optimization. *Journal of Biomechanics*. Volume 44, Issue 9, 3 June 2011, Pages 1722–1728
10. William R. Thompsona, Clinton T. Rubinb, Janet Rubina. Mechanical regulation of signaling pathways in bone. *Gene*. Volume 503, Issue 2, 25 July 2012, Pages 179–193
11. D.M. Brunette, M. Textor, P. Thomsen. *Titanium in Medicine. M. Science, Surface Science, Engineering, Biological Responses and Medical Applications.*(2001).ISBN: 978-3-642-631191
12. H.Y. Kim, Y. Ohmatsu, J.I. Kim, H. Hosoda, and S. Miyazaki. Mechanical properties and shape memory behaviour of Ti-Nb alloys. *Mater. Trans.*, 2004, vol. 45, pp. 1090–95.
13. T. Ozaki, H. Matsumoto, S. Watanabe, and S. Hanada. Beta TiNbSn alloys with low young's modulus and high strength. *Mater. Trans.*, 2004, vol. 45, pp. 2776–79.
14. M. Arciniegas, J. Peña, J.M. Manero, J.C. Paniagua, F.J.Gil. Quantum parameters for guiding the design of Ti alloys with shape memory and low elastic modulus. *Phil. Mag.* Vol. 88.2008, 2529–2548.
15. M. Arciniegas, J.M. Manero, J. Peña, F.J. Gil, J.A. Planell. Study of New Multifunctional Shape Memory and Low Elastic Modulus Ni-Free Ti Alloys. *Metall.Trans. A.* Vol. 39A, 2008. 743-751.

16. M. Arciniegas, J. Peña, F.J. Gil, J.M. Manero. In-vitro response of pre-osteoblastic MG63 cells on Ni-free Ti shape memory substrates. *Journal of Biomedical Materials Research: Part B - Applied Biomaterials*. Volume 101B, Issue 5, July 2013, pages 709–720.
17. Miyazaki S, Kim HY, Hosoda H. Development and characterization of Ni-free Ti-base shape memory and superelastic alloys. *Mater Sci Eng, A* 2006;438–440:18–24.
18. Hosoda H, Fukui Y, Inamura T, Wakashima K, Miyazaki S, Inoue K. Mechanical properties of Ti-based shape memory alloys. *Mater Sci Forum* 2003;426–432:3121–6.
19. Kim HY, Ikehara Y, Kim JI, Hosoda H, Miyazaki S. Martensitic transformation, shape memory effect and superelasticity of Ti–Nb binary alloys. *Acta Mater* 2006;54:2419–29.
20. M. González, J. Peña, J.M. Manero, M. Arciniegas, F.J. Gil. Optimization of the Ti-16.2Hf-24.8Nb-1Zr Alloy by Cold Working. *J. Materials Engineering and Performance*. Vol.18 2009. 506-10.
21. M. González, J. Peña, F.J. Gil, J.M. Manero. Low modulus Ti-Nb-Hf alloy for biomedical applications. *Materials Science & Engineering C*. Volume 42, 1 September 2014, Pages 691–695.
22. M. Ramalingam, A. Tiwari, H. Kobayashi. *Integrated Biomaterials for Biomedical Technology: Chapter 6: New kind of titanium alloys for biomedical applications*. John Wiley & Sons. 2012.
23. M. Morinaga and N. Yukawa, in *Computer-Aided Innovation of New Materials (CAMSE '90)*, M. Doyama et al. eds., Elsevier, North-Holland Inc., New York, p.803.
24. J.E. Carpenter, F. Weinhold. Analysis of the geometry of the hydroxymethyl radical by the “different hybrids for different spins” natural bond orbital procedure. *J. Molecular Structure: THEOCHEM*, Volume 169, 1988, Pages 41-62.
25. Gittens RA, Scheideler L, Rupp F, Geis-Gerstoffer J, Schwartz Z, Boyan BD. A review on the wettability of dental implant surfaces: Biological and clinical aspects. *Acta Biomater*. 2014;10:2907-18.
26. Hao Y.L., Li S.J., Sun S.Y., Zheng C.Y., Yang R. Elastic deformation behaviour of Ti–24Nb–4Zr–7.9Sn for biomedical applications. *Acta Biomater* vol 3 (2008) 277-286.
27. D.K. Owens, R.C. Wendt. Estimation of the surface free energy of polymers. *J. Appl. Polym. Sci* 1969, 13:1741-1747.
28. K.L. Mittal. *Advances in contact angle wettability and adhesion*. Vol 1. Scrivener publishing & Wiley. (2013) ISBN. 978-1-118-47292-7.
29. Hon, Y. H. & Wang Y.N, J. Y. and P. *Composition/Phase Structure and Properties of Titanium-Niobium Alloys*. *Mater. Trans.* 44, 2384 (2003).
30. H.Y. Kim, Y. Ikehara, J.I. Kim, H. Hosoda, S. Miyazaki. Martensitic transformation, shape memory effect and superelasticity of Ti–Nb binary changes in mechanical properties of Ti alloys in relation to alloying additions of Ta and Hf. *14th Int. Conf. Strength Mater.* 483-484, 153–156 (2008).
- [31] Zhou, Y.L., Niinomi, M. Akahori, T. Changes in mechanical properties of Ti alloys in relation to alloying additions of Ta and Hf. *14th Int. Conf. Strength Mater.* 483-484, 153–156 (2008).

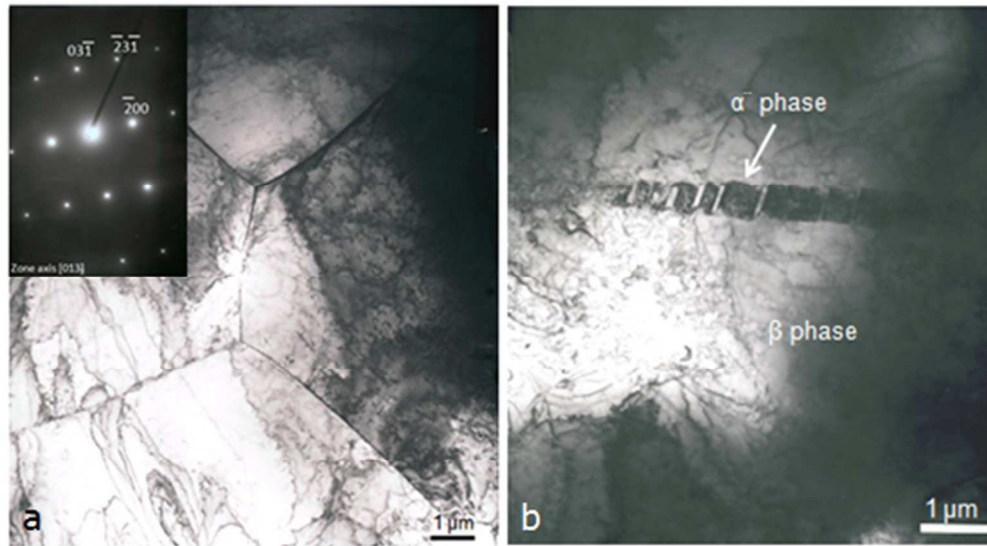
- 1
2
3 32. Hon, Y. H., Wang, J. Y. & Pan, Y. N. Influence of hafnium content on mechanical behaviors of
4 Ti-40Nb-xHf alloys. *Mater. Lett.* 58, 3182–3186. (2004).
5
6 33. D. De Fontaine and O. Buck. A Monte Carlo simulation of the omega phase transformation.
7 *Philos. Mag.* Vol 27, 1973 p697.
8
9 34. D. M. Brunette, P. Tengvall, M. Textor, P. Thomsen. Titanium in medicine: material science,
10 surface science, engineering, biological responses, and medical applications. ISBN: 978-3-642-63119-
11 1. (Springer, 2001).
12
13 35. Raabe, D., Sander, B., Friák, M., Ma, D. & Neugebauer, J. Theory-guided bottom-up design of L-
14 titanium alloys as biomaterials based on first principles calculations: Theory and experiments. *Acta*
15 *Mater.* 55, 4475–4487 (2007).
16
17 36. Nobuhito, S., Niinomi, M., Toshikazu, A., Takashi, S. & Tadahiko, F. Effects of Alloying
18 Elements on Elastic Modulus of Ti-Nb-Ta-Zr System Alloy for Biomedical Applications. *Mater. Sci.*
19 *Forum* 449-452, 1269–1272 (2004).
20
21 37. Zhou, Y.-L., Niinomi, M. & Akahori, T. Dynamic Young's Modulus and Mechanical Properties
22 of Ti-Hf alloys. *Mater. Trans.* 45, 1549 (2004).
23
24 38. Vasilescu E, Drob P, Raducanu D, Iordachescu D, et al. In vitro biocompatibility and corrosion
25 resistance of a new implant titanium base alloy. *J Mater Sci Mater Med.* (2010) 1959–68.
26
27 39. M. Long, H.J. Rack. Titanium alloys in total joint replacement—a materials science perspective.
28 *Biomaterials* 19 (1998) 1621—1639
29
30 40. Kobayashi, E., Wang, T.J., Doi, H., Yoneyama, T., and Hamanaka, H. Mechanical properties and
31 corrosion resistance of Ti-6Al-7Nb alloy dental castings. *J Mater Sci Mater Med.* 1998; 9: 567–574
32
33 41. Z. Cai, M. Koike, H. Sato, M. Brezner, Q. Guo, O. Okuno, T. Okabe. Electrochemical
34 characterization of cast Ti-Hf binary alloys. *Acta Biomaterialia*, Vol. 1, Issue 3, 2005, Pages 353-35
35
36 42. Wang XJ, Li YC, Lin JG, Yamada Y, Hodgson PD, Wen CE. In vitro bioactivity evaluation of
37 titanium and niobium metals with different surface morphologies. *Acta Biomater.* 2008; 4(5):1530-5.
38
39 43. Wang BL, Li L, Zheng YF. In vitro cytotoxicity and hemocompatibility studies of Ti-Nb, Ti-Nb-
40 Zr and Ti-Nb-Hf biomedical shape memory alloys. *Biomed Mater.* 2010 Aug;5(4):044102
41
42 44. M. Pegueroles, C. Tonda-Turo, J.A. Planell, F.J. Gil, C. Aparicio. Adsorption of Fibronectin,
43 Fibrinogen, and Albumin on TiO₂: Time-Resolved Kinetics, Structural Changes, and Competition
44 Study. *Biointerphases* (2012) 7:48
45
46 45. Hung A, Mwenifumbo S, Mager M, Kuna JJ, Yarovsky I, Stevens MM. Ordering surfaces on the
47 nanoscale: implications for protein adsorption. *J Am Chem Soc.* 2011;133(5):1438-50.
48
49 46. Anand G, Sharma S, Dutta AK, Kumar SK, Belfort G. Conformational transitions of adsorbed
50 proteins on surfaces of varying polarity. *Langmuir.* 2010 Jul 6;26(13):10803-11.
51
52 47. Arima, Y; Iwata, H. Effect of wettability and surface functional groups on protein adsorption and
53 cell adhesion using well-defined mixed self-assembled monolayers. *Biomaterials* 2007, 3074-3082.
54
55
56
57
58
59
60

1
2
3
4
5
6
7
8
9
10
11
12
13
14
15
16
17
18
19
20
21
22
23
24
25
26
27
28
29
30
31
32
33
34
35
36
37
38
39
40
41
42
43
44
45
46
47
48
49
50
51
52
53
54
55
56
57
58
59
60

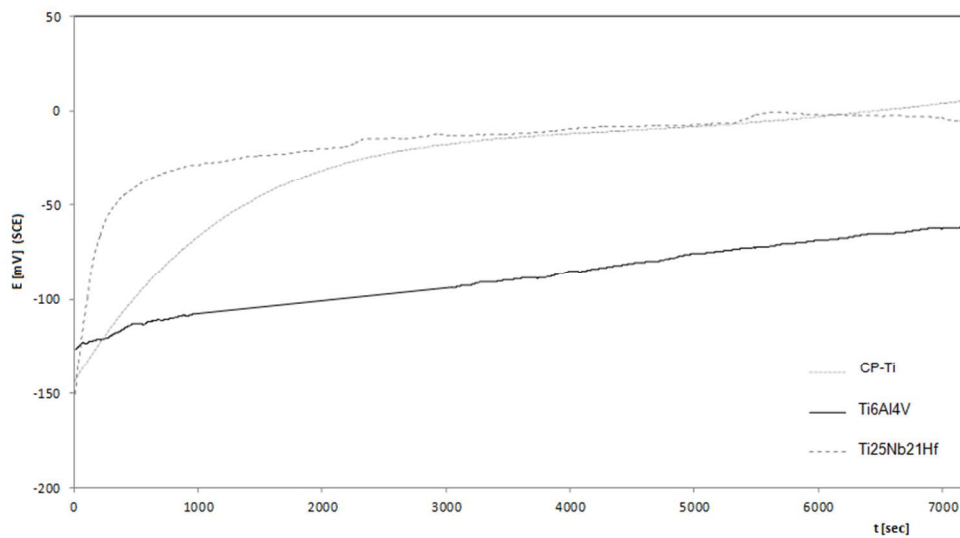


XRD pattern of Ti25Nb21Hf alloy
84x74mm (96 x 96 DPI)

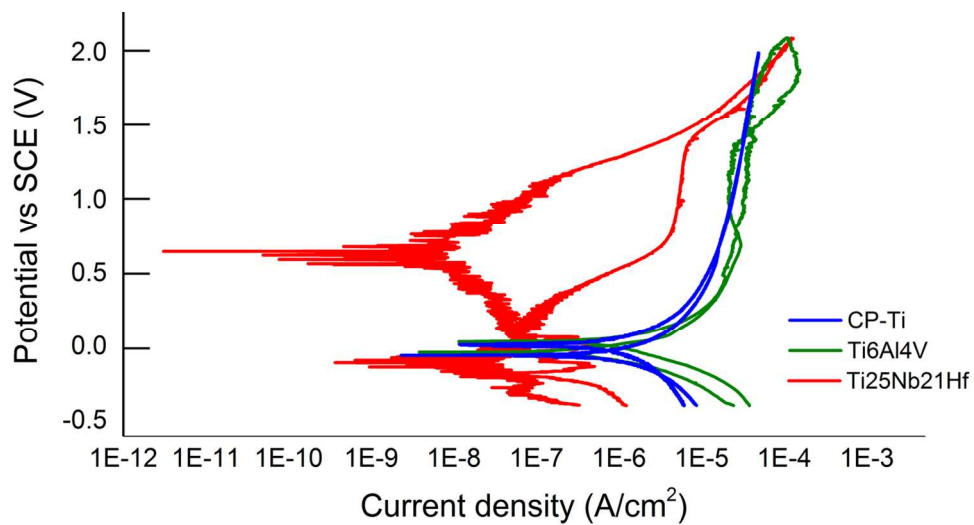
Peer Review



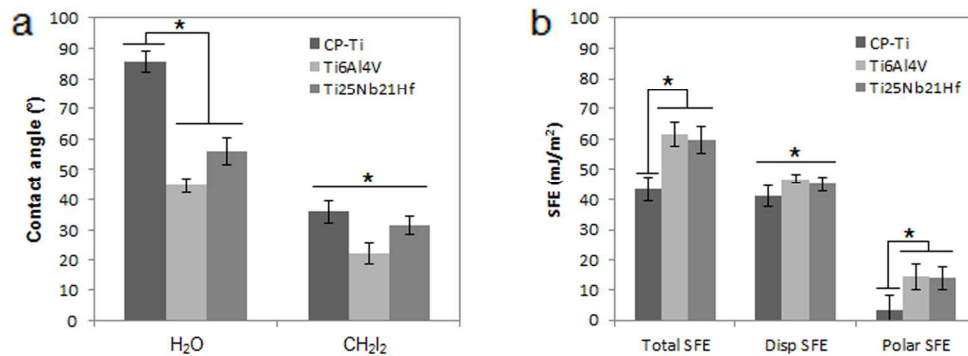
TEM images of the Ti₂₅Nb₂₁Hf alloy. Zone axis [013].
147x81mm (96 x 96 DPI)



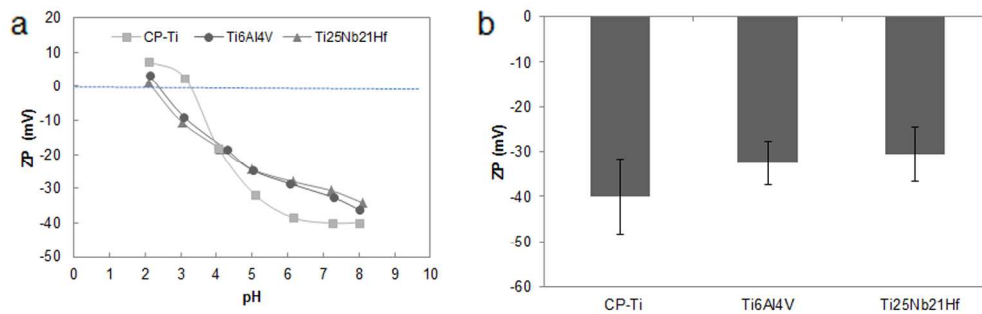
Open-circuit electrode potential as a function of time for the three materials under study in Hank's Balanced Salt Solution at 37°C
73x40mm (300 x 300 DPI)



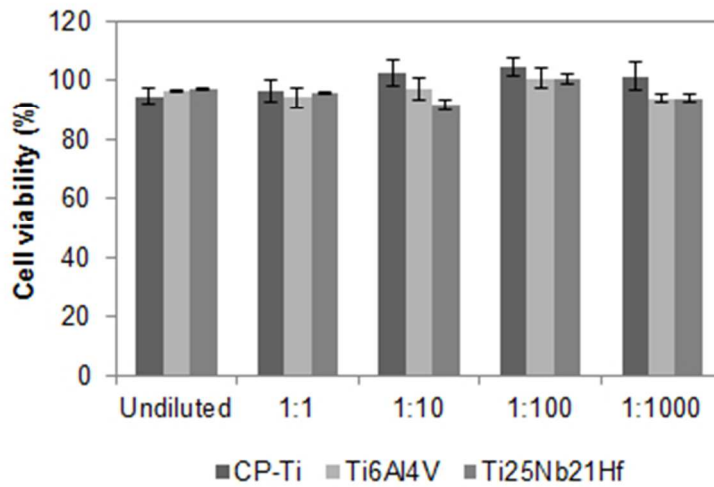
Cyclic voltammetry curves of Ti and Ti6Al4V and Ti25Nb21Hf alloys.
130x68mm (300 x 300 DPI)



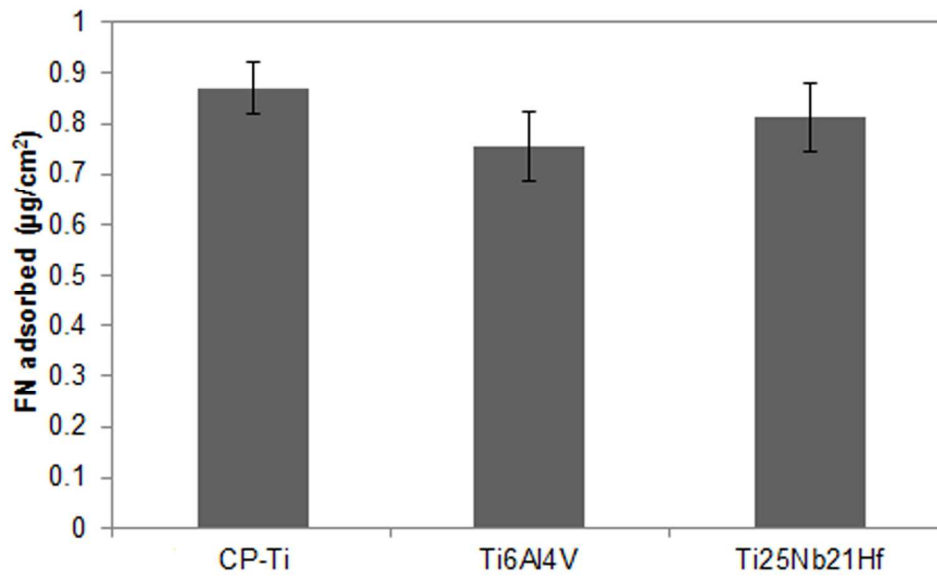
(a) Contact angles for water (H₂O) and diiodomethane (CH₂I₂) and (b) total surface free energy (SFE), dispersive (Disp) and polar components of SFE of Ti and Ti6Al4V and Ti25Nb21Hf alloys. The asterisk means differences between samples with $p < 0.05$.
189x69mm (300 x 300 DPI)



(a) pH dependence of the zeta-potential for Ti, Ti6Al4V and TiNbHf in a KCl electrolyte with a concentration 1mM (a) and (b) Zeta-potentials of the different samples at pH 7 (b).
276x89mm (300 x 300 DPI)

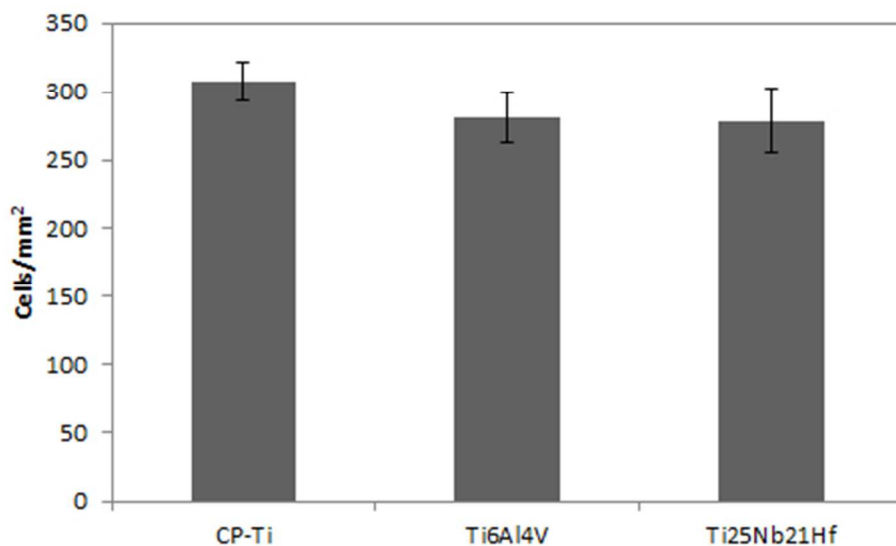


Cell viability of rMSCs after 24h exposure with different extract dilutions.
104x75mm (96 x 96 DPI)



Fibronectin adsorption onto the different tested materials after 2h of incubation at room temperature
126x76mm (300 x 300 DPI)

1
2
3
4
5
6
7
8
9
10
11
12
13
14
15
16
17
18
19
20
21
22
23
24
25
26
27
28
29
30
31
32
33
34
35
36
37
38
39
40
41
42
43
44
45
46
47
48
49
50
51
52
53
54
55
56
57
58
59
60



Adhesion of rMSCs (cells/mm²) onto the three tested materials.
127x76mm (96 x 96 DPI)

Peer Review

Phase	hkl	d (nm)	2 θ	I (%)
α''	200	0.24431	36.757	24
α''	002	0.23869	37.655	33
β	110	0.23466	38.326	100
α''	111	0.23078	38.997	100
α''	201	0.21748	41.488	14
α''	202	0.17073	53.639	14
β	200	0.16596	55.31	12
α''	113	0.13624	68.86	20
β	211	0.13507	69.542	17
β	220	0.11712	82.25	4
β	310	0.10459	94.868	5

1
2
3
4
5
6
7
8
9
10
11
12
13
14
15
16
17
18
19
20
21
22
23
24
25
26
27
28
29
30
31
32
33
34
35
36
37
38
39
40
41
42
43
44
45
46
47
48
49
50
51
52
53
54
55
56
57
58
59
60

Alloy	E (GPa)	σ_{max} (MPa)	σ_y (MPa)
CP-Ti	120 ± 16	550 ± 2.5	392 ± 34,5
Ti6Al4V	158 ± 8	986 ± 8	975 ± 47
Ti25Nb21Hf	85 ± 2	908 ± 14	816 ± 16

For Peer Review

Material	$E_{\text{open circuit}}$ [mV]
CP-Ti	2.5 ± 15
Ti6Al4V	-58 ± 4
Ti25Nb21Hf	-6 ± 15

For Peer Review